Investigation of the Unbalanced Magnetic Pull Damping Effect in Squirrel Cage Induction Machines

Investigation of the Unbalanced Magnetic Pull Damping Effect in Squirrel Cage Induction Machines

H. Chuan[*], *J. K. H. Shek*

Institute for Energy Systems, School of Engineering, The University of Edinburgh, United Kingdom

*H.Chuan@ed.ac.uk

Abstract: Unbalanced Magnetic Pull (UMP) in squirrel cage induction machines (SCIMs) is much lower than in wound rotor induction machines (WRIMs) when running below its rated slip. The difference in UMP is due to the UMP damping effect caused by the counteracting flux produced by the parallel-connected rotor bars of SCIMs. The UMP damping effect is comprehensively discussed by comparing the UMP and air-gap flux of both SCIMs and WRIMs. Subsequently, a UMP damping coefficient is proposed to be included in the conventional UMP analytical model, where the damping of UMP caused by the counteracting flux can be taken into account. Lastly, the UMP of the SCIM at different excitation frequencies and rotor resistance are investigated, which is used to verify the UMP damping effect.

1. Introduction

Unbalanced Magnetic Pull is caused by the uneven magnetic flux distribution around the machine. This can be caused by many factors, such as winding faults, uneven magnetisation of the iron core, broken bars, and rotor eccentricity [1]. UMP caused by rotor eccentricity is discussed in this paper since 80% of mechanical defects may cause rotor eccentricity [2]. In addition, rotor eccentricity may even occur in a newly-manufactured machine, where typically 10% of rotor eccentricity is permissible during the manufacturing stage [3].

In general, there are two main types of rotor eccentricity when axial variation is not considered; these are static and dynamic eccentricity. In practice, both types of eccentricity could exist together, known as mixed eccentricity [3]. For static eccentricity, the rotor rotates on its own axis but not in the centre of the stator bore (see Fig. 1(a)) [4], which is mainly caused by stator core ovality or incorrect positioning of the rotor and the stator during the assembling stage [5]. For dynamic eccentricity, the rotor is at the centre of the stator bore but does not rotate on its own axis (see Fig. 1(b)) [4], which can be caused by a bent shaft, mechanical resonances at critical speed, and bearing wear [6].

As UMP is a function of the degree of eccentricity and induction machines generally possess smaller air-gap, the UMP of induction machines is sensitive to rotor misalignment [7]. UMP caused by manufacturing tolerances accelerates bearing wear, which may lead to larger eccentricity that in turn causes larger UMP, resulting in a snowball effect. Bearing failure will cause rotor-to-stator rub, which may further damage the stator core and windings [3]. An induction machine failure survey reported that bearing related failure accounts for 40% of the total failures, while bearing failures can reach as high as 95% of the total failures when operated in harsh environments [8]. Therefore, understanding the characteristics of UMP could help in the design of machines, in which the UMP caused by manufacturing error or bearing wear can be taken into account.

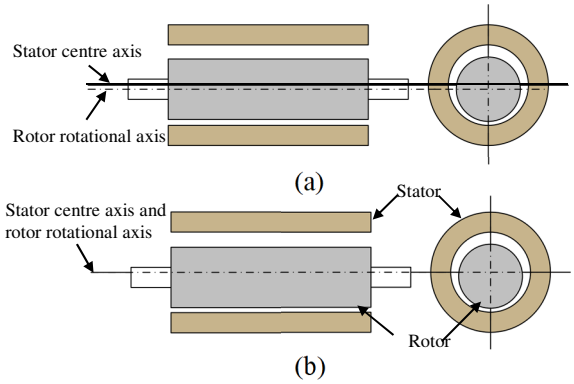

Fig. 1. *Cross-sectional view of the rotor with (a) static eccentricity, (b) dynamic eccentricity [4].*

In a healthy cylindrical machine, the uneven magnetic flux distribution caused by rotor eccentricity can be mathematically represented by two magnetic flux waves with pole-pairs differing by one for each space harmonic of the magnetic flux wave [9]. For a machine with p-pole pairs, the UMP is produced by the interaction between the p-pole pair flux wave and the $p \pm 1$ pole pair flux wave.

To calculate the UMP of induction machines, the vector of both the stator and rotor MMF are needed. Therefore, numerical methods need to be used to find the UMP of SCIMs, as the circulating current in the rotor bars is induced by the stator flux [10]. To include the damping effect caused by the rotor circulating current in the analytical calculation, a damping coefficient in the UMP calculation was first proposed in [11]. In [12], the authors proposed the use of effective eccentricity in the UMP calculation, which is a function of the damping coefficient. However, both papers lack verification from either experimental work or Finite Element Analysis (FEA). Furthermore, from existing literature it is apparent that investigation into the use of a damping coefficient is relatively unexplored.

In [13], in order to compare results from different literatures, a UMP factor is introduced to normalise the UMP of different induction machines. It is presented in the paper that the UMP in induction machines with a parallel path have

a much smaller UMP than those without a parallel path. When there is a parallel circuit in the machine, the counteracting flux wave can be induced to damp the existing $p \pm 1$ pole pair flux wave caused by rotor eccentricity. The parallel circuit can either be at the stator or the rotor. As the rotor bars of a SCIM are naturally parallel connected, the UMP is considerably lower than WRIMs [14]. In [15], the authors showed that the UMP of WRIMs can be 300% to 400% higher than SCIMs when operated below its rated slip. Furthermore, it has also been shown that UMP can be reduced by using parallel-connected stator windings [16] [17] [18]. Although the effectiveness of UMP damping is affected by the number of parallel stator windings, Dorrell et al. pointed out that parallel windings in the stator will generate a pulsating UMP vibration [17].

The radial force of the rotor is only caused by the magnetic flux that crosses the air-gap. In addition, not all the magnetic flux from the stator winding could be damped by the cage rotor, as the counteracting flux wave can only be produced when the magnetic flux wave cuts through the rotor bars. Therefore, UMP damping is mainly applicable for the fundamental magnetising flux [19]. The authors had previously shown that the magnetic flux wave can be categorised into the fundamental magnetising flux wave and the air-gap leakage flux wave (or higher harmonics flux wave) to calculate the UMP [20].

The air-gap leakage flux wave has higher space harmonics content, which include higher winding harmonics and rotor slots harmonics [20] [21]. The slot harmonics is mainly influenced by the slot magnetomotive force (MMF), where the slot permeance variation has little effect on the rotor slot harmonics flux wave [22]. Therefore, the slot permeance effect can be neglected, and the effective air-gap length can be modified by using the Carter factor [23]. Although the slotting effect can cause vibrations, it does not generate significant UMP. In [19] the authors demonstrated, with the use of FEA, that closing the rotor or stator slots does not reduce the UMP.

The air-gap is dominated by the fundamental flux wave when the induction machine operates below its rated slip. The air-gap is also dominated by the higher harmonics flux wave during start-up [21]. As higher harmonics flux waves are dominant at high slip, the UMP damping effect is negligible at machine start-up.

The objective of this paper is to investigate the UMP damping effect caused by the circulating current in the rotor bars. A UMP damping coefficient is proposed, which can be included in the conventional UMP analytical model. This paper is organised as follows. In Section 2, the formation of UMP is discussed. The setup for FEA and experimental work are then presented in section 3. Section 4 shows the difference between SCIMs and WRIMs. In Section 5, the derivation and verification of the proposed damping coefficient is presented. Finally, the UMP damping effect at different operating conditions are shown in Section 6, with conclusions given in Section 7.

2. Background

2.1. Rotor Eccentricity

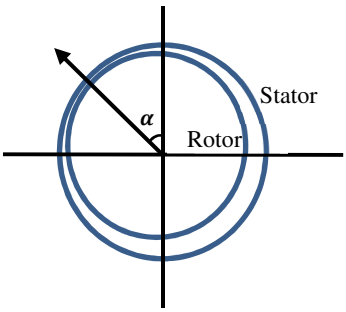

Fig. 2 shows a rotor with eccentricity, where α is the angle of the narrowest air-gap.

Fig. 2. *Cross section of an eccentric rotor*

Assuming that the percent of rotor eccentricity is small compared to the radius of the rotor, the air-gap perpendicular to the eccentricity angle has the same air-gap as a concentric rotor. The air-gap, g', for an eccentric rotor is [23]:

$$g'(\theta, t) = g_0(1 - \varepsilon\, cos(\theta - \alpha)) \tag{1}$$

where g_0 is the mean air-gap length, θ is the angle around the circumference, α is the angle of the narrowest air-gap, and ε is the degree of eccentricity, which is the ratio between the length of the eccentric rotor displacement from the centre axis and the air-gap length of the concentric rotor.

In (1), both ε and α are a function of time, degree of eccentricity, which is illustrated in Fig. 3, where the subscript s and d refer to the static and dynamic eccentricity respectively, ω_r is the rotor angular frequency (rad/s), α_d refers to the angle that is relative to the angle of static eccentricity at time $= 0$.

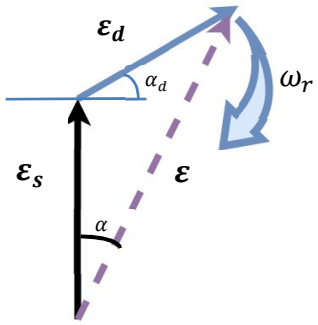

Fig. 3. *Cross section of an eccentric rotor*

Let the angle of the static eccentricity be 90°. The instantaneous degree of eccentricity is shown in (2), which is the vector summation of the degree of static and dynamic eccentricity.

$$\varepsilon = \sqrt{(\overline{\varepsilon_s} + \overline{\varepsilon_d}\sin(\omega_r t + \alpha_d))^2 + \left(\overline{\varepsilon_d}\cos(\omega_r t + \alpha_d)\right)^2} \tag{2}$$

As the angle of the narrowest air-gap is also a function of time and rotating frequency, the angle of the overall eccentricity will change if dynamic eccentricity exists. The angle of the narrowest air-gap can be derived as

$$\alpha = tan^{-1}\frac{\overline{\varepsilon_s} + \overline{\varepsilon_d}\, sin(\omega_r t + \alpha_d)}{\overline{\varepsilon_d}\, cos(\omega_r t + \alpha_d)} \tag{3}$$

$$\alpha = \left(\tan^{-1}\frac{\overline{\varepsilon_s}}{\overline{\varepsilon_d}\cos(\omega_r t + \alpha_d)}\right) + \omega_r t + \alpha_d \quad (4)$$

Refer to (4), the angle of the narrowest air-gap for a mixed eccentricity case is a function of the rotor angular frequency and the ratio between the static and the dynamic eccentricity. Therefore, the angle of the narrowest air-gap of the machine does not linearly change with time.

2.2. UMP Calculation

As the stator and rotor core are assumed to have infinite permeability, the permeance of the magnetic path is equal to the air-gap permeance, Λ. The air-gap permeance at each point around the rotor is [24]:

$$\Lambda = \frac{\mu_0}{g'(\theta,t)} = \frac{\mu_0}{g_0(1-\varepsilon cos(\theta-\alpha))} \quad (5)$$

For low degree of eccentricity, it is assumed that the magnetic permeance has a linear relationship with the degree of eccentricity [14], hence air-gap permeance can be written as:

$$\Lambda = \frac{\mu_0}{g_0}(1+\varepsilon cos(\theta-\alpha)) \quad (6)$$

The magnetic flux around the air-gap can be found by multiplying the magnetic permeance with the MMF around the air-gap [25], where J is the stator MMF:

$$B\ (\theta,t) = \Lambda J \quad (7)$$

The magnetic flux around the air-gap caused by low degree of rotor eccentricity is shown in (8) [23].

$$\begin{aligned} B &= \sum_{p=1}^{\infty} B_p cos(\omega t + p\theta) \times \left(1 + \varepsilon_s cos(\theta-\alpha_s) + \varepsilon_d \cos(\omega_r t - \alpha_d)\right) \\ &= \sum_{P=1}^{\infty}\Big[B_p \cos(\omega t + p\theta - \alpha) + \frac{1}{2}B_p\varepsilon_s \cos(\omega t + (p-1)\theta - \alpha_s) \\ &\quad + \frac{1}{2}B_p\varepsilon_s \cos(\omega t + (p+1)\theta - \alpha_s) \\ &\quad + \frac{1}{2}B_p\varepsilon_d \cos((\omega-\omega_r)t + (p-1)\theta + \alpha_d) \\ &\quad + \frac{1}{2}B_p\varepsilon_d \cos((\omega+\omega_r)t + (p+1)\theta - \alpha_d)\Big] \end{aligned} \quad (8)$$

where ω is the angular excitation frequency (rad/s), B is the magnetic flux density (T), ω_r is the rotor rotational angular frequency (rad/s) and p is the order of space harmonic.

The first term in (8) is the magnetic flux wave of a healthy machine. The second and third terms represent the additional $p \pm 1$ pole pair flux wave which is caused by static eccentricity. The fourth and fifth terms represent the additional $p \pm 1$ pole pair flux wave which is caused by dynamic eccentricity. In general, the magnitude of the additional $p \pm 1$ pole pair flux wave is a function of magnetic flux density of a concentric rotor (B_p) and the degree of eccentricity (ε).

$$UMP = rL\sum_{p=1}^{\infty}\int_0^{2\pi}\frac{B^2}{2\mu_0}\cos(\theta)\,d\theta \quad (9)$$

To find the UMP exerted on the rotor, integration of the Maxwell Stress Tensor around the air-gap is used to find the nett radial force [17], as shown in (9). Equation (10) shows the UMP caused by the rotor eccentricity, where detail derivation is shown in [26].

$$\begin{aligned} UMP = \frac{\pi rL}{2\mu_0}\sum_{p=1}^{\infty} {B_p}^2[\varepsilon_s(1+\cos(2\omega t)) \\ + \varepsilon_d(cos(\omega_r t + \alpha_r) + cos(2(\omega+\omega_r)t + \alpha_d))] \end{aligned} \quad (10)$$

From (10), the UMP caused by either the static or dynamic eccentricity consists of 2 components, where the first component is caused by the interaction between two flux waves with the same rotational direction. The second component is produced by the interaction between two flux waves with the opposite rotational direction [25]. The second component is negligible because the backward rotational flux wave is relatively small for an induction machine with a series-connected stator winding and balanced three phase supply.

3. Simulation and experimental setup

3.1. FEA Setup

A 2D-FEA was carried out using MagNet FEM software by Infolytica. 2D-FEA assumes that there is no changes in the axial direction of the machine. Then, the end winding resistance and inductance are added to the circuit as a lumped resistance and inductance. As the machine with rotor eccentricity is not symmetry, the full model of the machine needs to be used.

Transient with Motion solver with 100 time steps per period of excitation frequency is used. Non-linear magnetic property is selected in the simulation, and it is solved with Newton-Raphson convergence method. Time-stepping simulation is used because it is able to model all the time harmonics of the magnetic flux distribution in the machine, which also take into account the induced MMF caused by the flux harmonics [27].

For the meshing in FEA, choosing the optimised mesh size is crucial to obtain accurate results with lesser time consumed. The mesh size is varied depending on the geometry and the material complexity, in which finer mesh size is used at the air-gap region and the corner of the geometry. In [28], the author had shown the solution of FEA is sensitive to the meshing of air-gap. Movement or distortion of the mesh in the air-gap would lead to undesirable remeshing noise [29]. Therefore, a smaller mesh size is used in the air-gap to increase the accuracy of the solutions. Then, Moving-band technique is used to prevent the air-gap to be re-meshed at every time step, which is time consuming. An additional layer is added in between the stationary part and the rotational part, so the air-gap is divided into 3 sections, which are shown in Fig. 4. Therefore, only the moving band layer is re-meshed at every time step while the rotor is rotating.

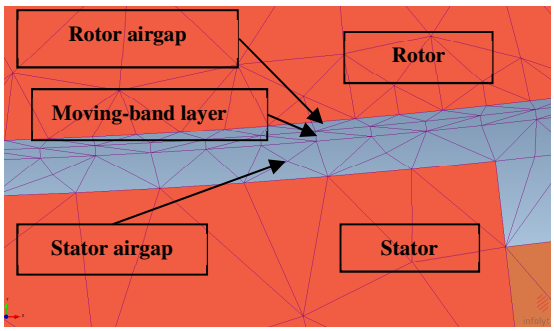

Fig. 4. *Cross section of an eccentric rotor*

Table 1 shows the 3 induction machines parameters that will be used in this paper, and Fig. 5 shows the meshed model of the 3 induction machines in FEA. The 8-pole SCIM parameter is based on the experimental model which is used to verify the UMP Damping Coefficient in Section 5 and to investigate UMP of different excitation frequency in Section 6. The 4-pole WRIM and SCIM are used to compare the UMP in Section-4. Then, the 4-pole SCIM is used to examine the effect of rotor resistance in Section 6.

Table 1 Machine Parameters

	8-pole SCIM	4-pole WRIM	4-pole SCIM
Power, kW	5.5	7.5	7.5
Number of poles	8	4	4
Axial length, mm	180	178.6	178.6
Stator diameter, mm	120	140	140
Rotor diameter, mm	78	89.75	89.75
Air-gap length, mm	0.9	0.5	0.5
Stator slot number	52	36	36
Stator turns per coil	13	22	22
Stator phase resistance, Ohm	1.579	1.08	1.08
Stator's parallel winding	1	1	1
Rotor slot number	42	48	28
Rotor turns per coil	1	6	1
Rotor phase resistance, Ohm	0.85	1.3	1.1
Stator phase inductance, H	0.1795	0.28	0.28
Leakage factor	0.18	0.12	0.11
Rotor inertia, kg/m^2	0.0804	0.1296	0.1296

3.2. Experimental Setup

Experimental work was carried out on the 8-pole 5.5 kW SCIM. The overview of the experimental setup is shown in Fig. 6(a). The permanent magnet machine acts as a generator which is connected to the rotor via torque transducer. The back-to-back connected electrical machines is shown in Fig. 6(b), where the SCIM was tested as a motor. The test motor is controlled by using an inverter. Then, the data collected from the force plate is send to the data acquisition (Dynoware 5697) through charge amplifier, and 1000 Hz sampling frequency is used.

As UMP is the attraction force between the stator and the rotor, in order to measure the UMP, the stator and rotor need to be separated and mounted on different platforms. Therefore, the stator is mounted on the force table, and the rotor is attached to a bearing holder which is mounted on the test rigs (see Fig. 6(c)). The force table is built with an aluminium plate and 4 force sensors (Kistler 9366C).

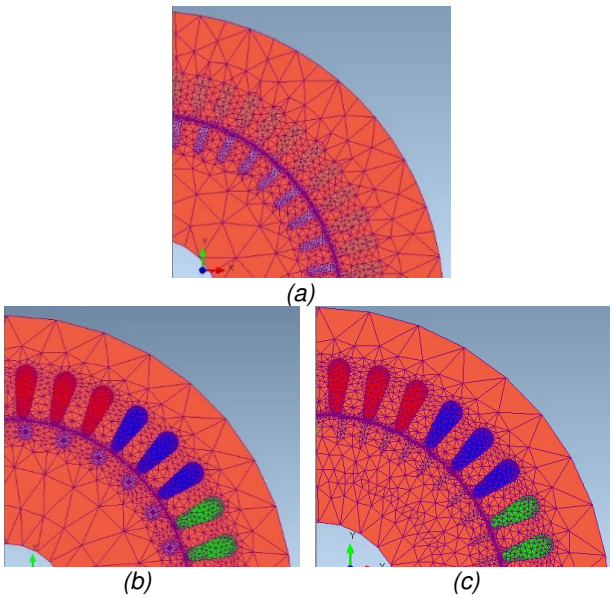

Fig. 5. *Models under meshed view in FEA: (a) 8-pole SCIM, (b) 4-pole SCIM (c) 4-pole WRIM.*

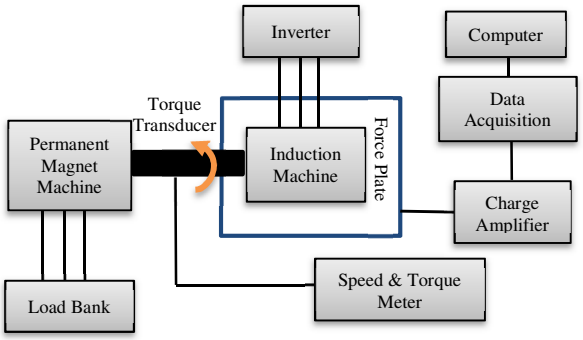

(a)

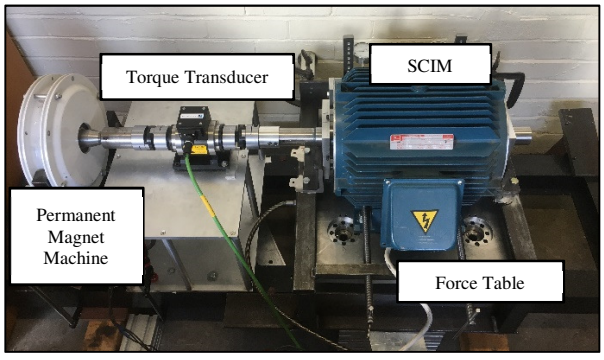

(b)

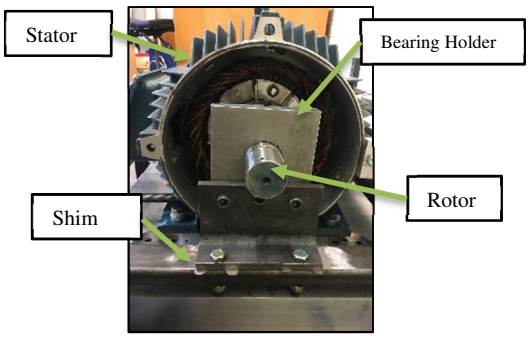

(c)

Fig. 6. *Experimental work setup: (a) overview (b) motor-generator test rig front view (c) side view*

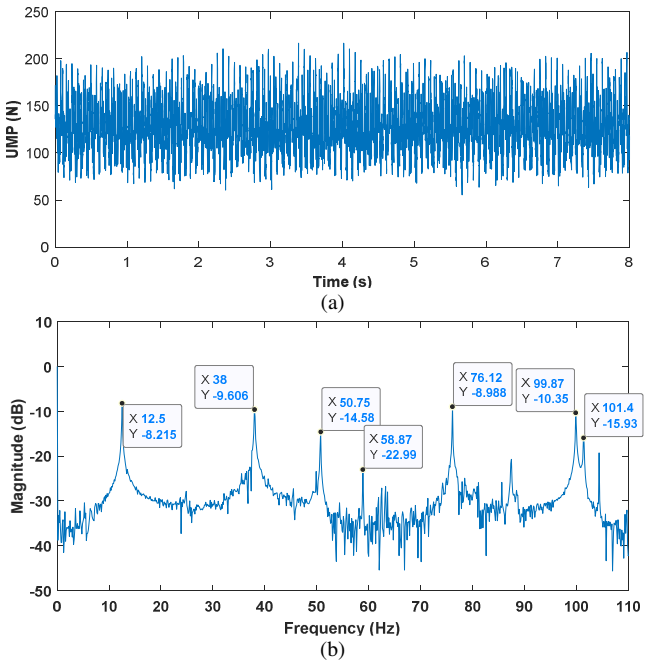

Fig. 7. *UMP of 50% eccentricity at no-load with 0.5 pu voltage: (a) measurement (b) FFT analysis*

In this paper, the UMP damping effect of SCIM with static eccentricity will be investigated. To create the static eccentricity, shims were added under the bearing holder, as shown in Fig. 6(c). The length of the rotor displacement from the centre of the stator bore is based on the thickness of the shims. Once the eccentricity is created, a feeler gauge was used to validate the air-gap length around the rotor.

As an example, Fig. 7(a) shows the UMP measurement when the SCIM is not loaded. It has shown that the data has different harmonics contents. Therefore, Fourier analysis was performed to extract the useful information, which is illustrated in Fig. 7(b). From (10), UMP caused by static eccentricity has a constant component (0 Hz) and a 2-times supply frequency component (~100Hz). The Fourier analysis shows that the dominant force component is the constant component, and the 2-times supply frequency component, which is the 101 Hz (see Fig. 7(b)). As the backward rotating flux wave is negligible in a SCIM with series-connected stator winding and a balanced three phase supply, the 2-times supply frequency component is negligible [25]. Meanwhile, noise from the mechanical coupling should also be neglected, which include the 12.5 Hz rotational frequency components and other harmonics component from the rotor frequency (38 Hz, 50 Hz, 76 Hz, 99.87 Hz).

4. Comparison of SCIM and WRIM

Based on the rotor winding configuration, induction machines can be divided into SCIM and WRIM. Typically, the SCIM has a parallel-connected rotor bar (see Fig. 8 (a)), in which the current in every rotor bar can be different, while the WRIM has a series connected rotor winding (see Fig. 8 (b)), in which the same current flows in the rotor winding of the same pole.

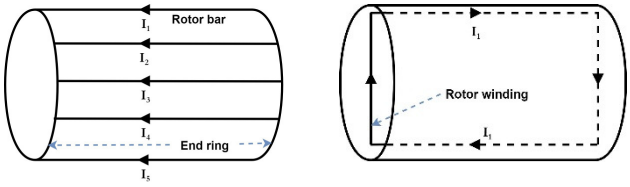

Fig. 8. *Rotor winding configuration: (a) cage rotor (parallel-connected), (b) wound rotor (series-connected).*

For the parallel-connected rotor bar of SCIM, electromotive force can be induced by wide range of magnetic flux waves from different space harmonics. This characteristic allows circulating current to flow in parallel-connected rotor bars to damp the additional $p \pm 1$ pole pair stator flux wave, in which the UMP can also be damped. However, the damping of UMP is less significant for magnetic flux waves with higher space harmonics [21]. Meanwhile, the series-connected rotor winding of WRIM can only be induced by the magnetic flux wave with the fundamental pole pair harmonics group. Therefore, there is no damping of UMP in WRIM [14].

The comparison between SCIM and WRIM in this section is based on FEA, where the 4-pole WRIM and 4-pole SCIM is used. The rotor is set at 50% static eccentricity towards the negative y-axis direction, with an excitation voltage of 400 V and 50 Hz at no-load.

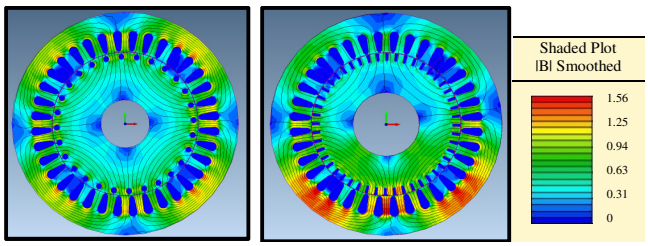

Fig. 9. *Magnetic flux density distribution: (a) 4-pole SCIM (b) 4-pole WRIM.*

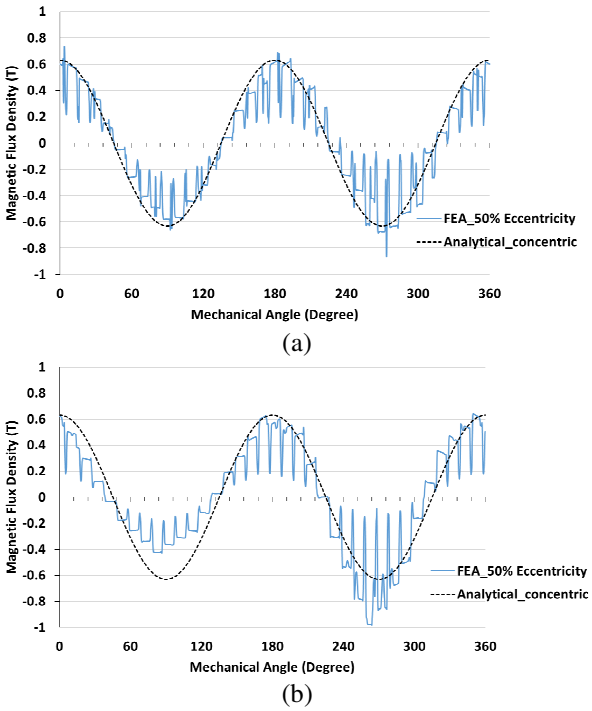

Fig. 10. *UMP of WRIM and SCIM at different slip.*

Fig. 9 shows the magnetic flux density distribution of both machines at no-load operation, where the WRIM has a higher magnetic flux density than SCIM around the negative *y*-axis area. The magnetic flux density around the air-gap in Fig. 9 is plotted at Fig. 10, and they are compared with the fundamental magnetising flux wave (dotted line). The SCIM has a more evenly distributed magnetic flux than the WRIM, because the additional $p \pm 1$ pole pair flux wave was damped by the cage rotor bar. As the direction of the narrowest air-gap is at 270°, the magnetic flux density of WRIM at around 270° is higher than the magnetic flux density at around 90°.

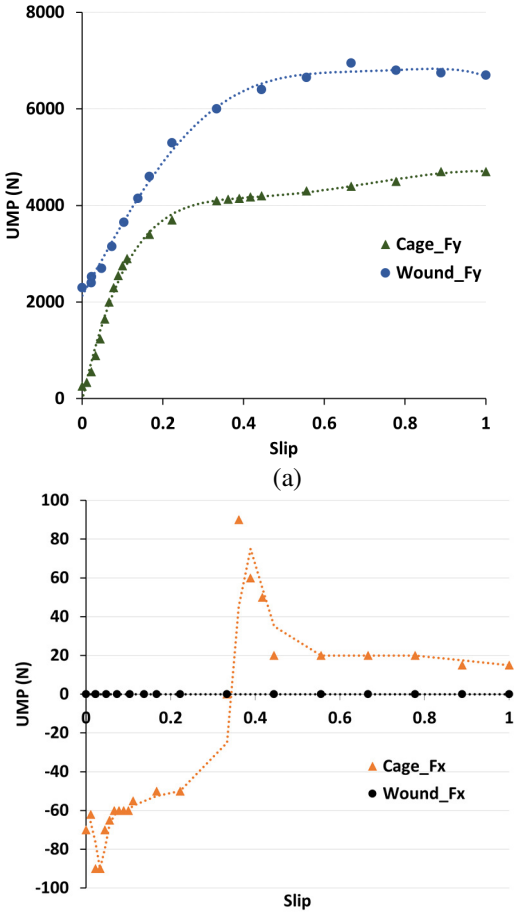

Fig. 11. *UMP of WRIM and SCIM at different slip.*

From Fig. 11(a), for both WRIM and SCIM, the *y*-axis UMP increases as the slip increases because more leakage flux crosses the air-gap when the rotor slip is larger, which leads to larger UMP. The UMP is proportional to the square of magnetic flux density, as shown in (10). When UMP damping effect is not considered, the UMP characteristic is correlated with the current because magnetic flux density is linearly proportional to the current. For the *y*-axis UMP, the WRIM has a higher UMP than the SCIM at every operating point. The difference in UMP mainly comes from the damping effect of the parallel-connected rotor bar of SCIM.

For SCIM, the damping of UMP has a non-linear relationship with rotor slip [20]. For a 2-pole pair SCIM, the damping of UMP is least effective when the rotor is running at 0.33 rotor slip. When the SCIM is excited with 50 Hz frequency, the rotor speed of the 2-pole pair SCIM at 0.33 rotor slip is 1000 RPM, which is the same as the synchronous speed of the 3-pole pair flux wave caused by rotor eccentricity. Therefore, at 0.33 slip, the 3-pole pair harmonic flux wave is not damped, as rotor current is not induced.

From 0 slip to 0.33 slip, the increment rate of UMP in the SCIM is higher than the WRIM, which is caused by the reduction of the UMP damping effect. Then, from 0.33 slip to 1 slip, the UMP difference between SCIM and WRIM increases because the effectiveness of the damping effect increases. The effectiveness of damping effect will be further discussed in Section 5.

When there is no damping of UMP, the x-axis UMP should be 0 because the rotor eccentricity is set towards the y-axis direction. Therefore, the WRIM's x-axis UMP is almost zero at different slip (see Fig. 11(b)). Meanwhile, the SCIM's x-axis UMP changes with slip, and the direction of UMP changes at around 0.33 slip. The change of UMP direction is due to the 3 pole-pair flux wave changes from lagging to leading the rotor at 1000 RPM, which is the synchronous speed of 3 pole-pair flux wave.

5. UMP Damping Effect

5.1. Derivation for the Damping Coefficient

The damping effect is investigated through analysing the counteracting flux wave produced by the rotor, as the damping effect is less significant for magnetic flux wave with higher space harmonics [21]. Therefore, only the fundamental magnetising flux wave will be investigated in this paper, where $\boldsymbol{\lambda}_s{}^{p}$ is the fundamental magnetising flux wave, $\boldsymbol{\lambda}_s{}^{p\pm1}$ is the sideband flux wave which is caused by rotor eccentricity, and $\boldsymbol{\lambda}_r{}^{\boldsymbol{p\pm1}}$ is the counteracting flux wave of the rotor. All the rotor parameters shown in this section are referred to the stator side.

When the rotating frequency of $\boldsymbol{\lambda}_s{}^{p\pm1}$ is different from the rotor rotating frequency, the $\boldsymbol{\lambda}_s{}^{p\pm1}$ induces a voltage across the rotor bar, the induced voltage is represented by the right-hand terms of (11).

$$\omega_{slip}{}^{p\pm1}\boldsymbol{\lambda}_s{}^{p\pm1} = \left(\sqrt{{R_r}^2 + (\omega_{slip}{}^{p\pm1}L_r)^2}\right) i_r \qquad (11)$$

where, ω_{slip} is the angular slip frequency, which is the angular frequency difference between the angular frequency of $\boldsymbol{\lambda}_s{}^{p\pm1}$ and the rotor angular frequency, i_r is the rotor current, R_r is the rotor resistance, and L_r is the rotor inductance.

Then, the current that flows in the rotor bar will produce $\boldsymbol{\lambda}_r{}^{\boldsymbol{p\pm1}}$, which is shown in (12). Interaction of $\boldsymbol{\lambda}_s{}^{p}$ and $\boldsymbol{\lambda}_r{}^{\boldsymbol{p\pm1}}$creates a counteracting force to damp the force that is caused by the interaction of $\boldsymbol{\lambda}_s{}^{p}$ and $\boldsymbol{\lambda}_s{}^{p\pm1}$.

$$\boldsymbol{\lambda}_r{}^{p\pm1} = L_r i_r \qquad (12)$$

Therefore, the damping effect can be determined by investigating the resultant vector between $\boldsymbol{\lambda}_r{}^{p\pm1}$ and $\boldsymbol{\lambda}_s{}^{p\pm1}$. The vector representation of the magnetic flux wave is shown in Fig. 11.

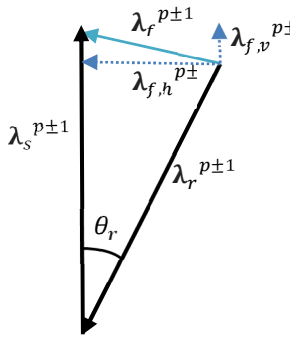

Fig. 12. *Vector representation of the* $\boldsymbol{\lambda}_s^{p\pm1}$ *and* $\boldsymbol{\lambda}_r^{p\pm1}$

The resultant magnetic flux, $\lambda_n^{p\pm1}$, which is the vector summation of $\boldsymbol{\lambda}_s^{p\pm1}$ and $\boldsymbol{\lambda}_r^{p\pm1}$, is shown in (13).

$$\lambda_n^{p\pm1} = \lambda_s^{p\pm1}\sqrt{1+\left(\frac{\omega_{slip}^{p\pm1}k_\sigma L_r}{\sqrt{R_r^2+(\omega_{slip}^{p\pm1}L_r)^2}}\right)^2 - 2\frac{\omega_{slip}^{p\pm1}k_\sigma L_r}{\sqrt{R_r^2+(\omega_{slip}^{p\pm1}L_r)^2}}\cos\theta_r} \quad (13)$$

where θ_r is angle difference between stator and rotor flux, and L_σ is the air-gap leakage inductance. As only the magnetic flux crosses the air-gap would produce attraction force between the stator and the rotor, the $\boldsymbol{\lambda}_r^{p\pm1}$ value is smaller when it is used to calculate the resultant flux that produced UMP. A flux coupling factor, k_σ, is introduced to reflect the percentage of the flux that crosses the air-gap, as shown in (14), with a value between 0 and 1.

$$k_\sigma = \frac{L_r - L_\sigma}{L_r} \quad (14)$$

The resultant magnetic flux in the air-gap is separated into the vertical component (15) and the horizontal component (16).

$$\lambda_v^{p\pm1} = \lambda_s^{p\pm1} - L_r\frac{\omega_{slip}^{p\pm1}k_\sigma\lambda_s^{p\pm1}}{\sqrt{R_r^2+(\omega_{slip}^{p\pm1^{p\pm1}}L_r)^2}}cos\theta_r \quad (15)$$

$$\lambda_h^{p\pm1} = -L_r\frac{\omega_{slip}k_\sigma\lambda_s^{p\pm1}}{\sqrt{R_r^2+(\omega_{slip}^{p\pm1}L_r)^2}}sin\theta_r \quad (16)$$

where, the subscript "v" and "h" are vertical and horizontal component respectively. UMP is produced by the interaction between magnetic flux wave with space harmonics difference by 1. As shown in (8), the magnitude of the resultant $p\pm1$ has a linear relationship with the total UMP produced for low degree of eccentricity case. Therefore, UMP Damping Coefficient, β, is proposed, which is the ratio between the resultant magnetic flux and the magnetic flux without any damping.

$$\beta = \frac{\boldsymbol{\lambda}_n^{p\pm1}}{\boldsymbol{\lambda}_s^{p\pm1}} \quad (17)$$

$$\beta = \sqrt{1+\left(\frac{\omega_{slip}^{p\pm1}k_\sigma L_r}{\sqrt{R_r^2+(\omega_{slip}^{p\pm1}L_r)^2}}\right)^2 - 2\frac{\omega_{slip}^{p\pm1}k_\sigma L_r}{\sqrt{R_r^2+(\omega_{slip}^{p\pm1}L_r)^2}}\cos\theta_r} \quad (18)$$

The UMP Damping Coefficient can be used to simplify the analytical calculation of the UMP caused by the fundamental magnetising flux, as it represents the resultant $p\pm1$ flux wave. From (8), the ε is the ratio between $p\pm1$ flux and p flux. To reflect the damping of UMP, an effective eccentricity, ε_{eff}, was previously used by [12]. The ε_{eff} introduced in this paper is shown in (19). The UMP Damping Coefficient has a linear relationship with ε_{eff}, which means the UMP is larger when the damping coefficient is higher.

$$\varepsilon_{eff} = \beta\varepsilon \quad (19)$$

In Fig. 13, the damping coefficients of SCIMs with three different pole numbers are calculated through (18). The SCIMs are assumed to have the same rotor time constant of 0.15 and leakage factor of 0.9. The excitation frequency of the SCIMs is 50 Hz, but the excitation voltage is not included because the saturation factor is neglected.

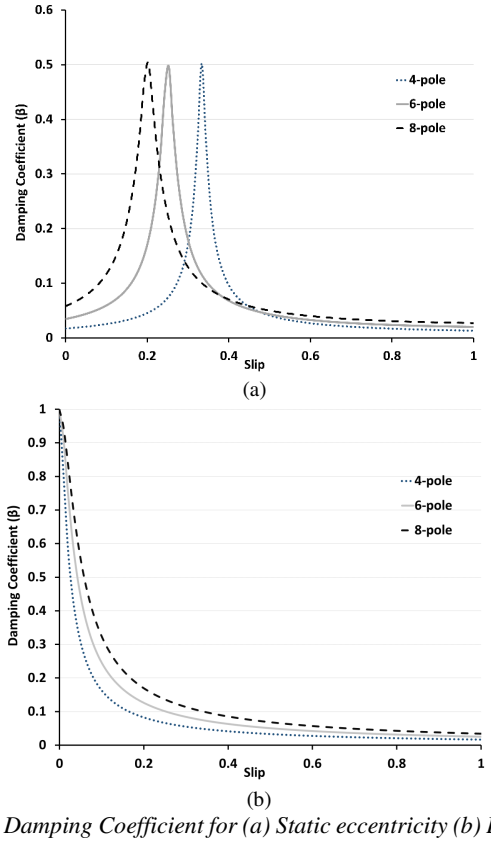

Fig. 13. *Damping Coefficient for (a) Static eccentricity (b) Dynamic eccentricity*

From Fig. 13(a), the spike of the damping coefficient of static eccentricity occurs at different slip values for different pole numbers. For example, in the 8-pole SCIM, the damping effect becomes least significant at 0.2 slip, because the *p+1* (5 pole-pair) flux wave does not induce voltage on the rotor. From (11), it shows that the rotor does not produce the counteracting flux wave to damp the 5 pole-pair flux wave when the slip frequency of the flux is 0. Therefore, there is a spike in the UMP Damping Coefficient.

Furthermore, higher pole pair number has a higher Damping Coefficient when the SCIM is running within its operating range (<0.05 slip), because the UMP Damping Coefficient is a function of slip frequency (not slip ratio). The additional $p\pm1$ pole pair flux waves of SCIM with higher

pole number have a lower slip frequency if compared to SCIM with lower pole numbers, which also means that the rotor reactance is lower, and the effectiveness of UMP damping effect reduces. Therefore, it can be concluded that SCIM with higher pole numbers has a larger UMP.

In Fig. 13(b), the damping coefficient of dynamic eccentricity decreases when the slip increases. At every rotor slip, the damping coefficient is smaller for SCIM with smaller pole pair number. The peak of damping coefficient for dynamic eccentricity is at 0 slip, because the $p \pm 1$ pole pair flux wave has the same rotational speed with the rotor, which can be seen from (8). Therefore, no EMF is induced at the rotor bars when it is not loaded.

5.2. Verification of the Damping Coefficient

To verify the proposed UMP Damping Coefficient, the UMP is calculated using (10) and (19), and it is compared with results from FEA and experimental work. The presented analytical results only includes the fundamental pole-pair magnetic flux wave.

Static eccentricity is used in this paper to verify the UMP Damping Coefficient. To examine the damping coefficient of the fundamental magnetising flux wave, a low excitation frequency of 10 Hz is chosen to be tested. This is because the magnetising flux wave is still the dominant flux at high rotor slip for low excitation frequency. In addition, to avoid magnetic saturation, the magnetising flux is set at 40% of the rated flux and the rotor is set to 10% static eccentricity towards the y-axis (vertical) direction.

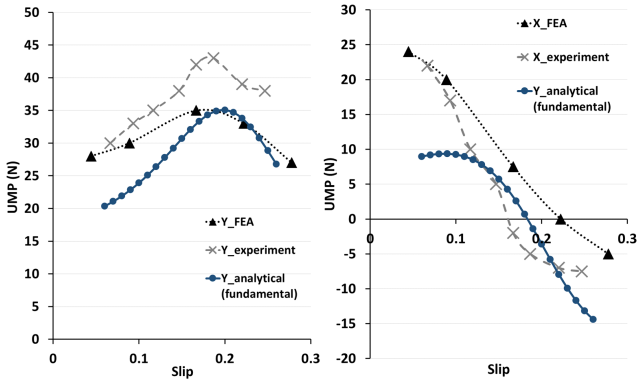

Fig. 14. *UMP for 8-pole SCIM at 10 Hz excitation frequency: (a) y-axis (b) x-axis*

Fig. 14 shows the comparison of UMP at 10 Hz excitation frequency with 10% eccentricity and 40% rated flux. As the rotor eccentricity is set towards the *y*-axis direction, the *y*-axis UMP always acts towards the same direction (see Fig. 14(a)). This can be proven using (15), where the sign of $\lambda_v^{p\pm1}$ will remain the same because (15) is a cos function, and also the rotor flux is induced by the stator flux, so θ_r is between -90° and +90°. Furthermore, the UMP calculated by the analytical model is slightly lower than the FEA and experimental results. This is because only the fundamental component of magnetising flux is considered in the analytical model.

Fig. 14(b) shows the *x*-axis UMP changes from positive to negative at around 0.2 slip. From (16), the damping coefficient of the *x*-axis is a sine function. Therefore, the direction of the UMP depends on whether the rotational speed of the rotor is lagging or leading the rotational of the additional $p \pm 1$pole-pair flux wave caused by eccentricity. The rotor flux wave induced by the 3-pole pair flux wave always lags the stator flux for all values of slip. However, the 5 pole-pair flux wave changes from leading to lagging after 0.2 slip.

In Fig. 14(b), we can see that there is an offset between the analytically calculated UMP with the FEA. This is due to the magnetising flux wave of the winding harmonics not being taken into account in the analytical model. In addition, the difference is bigger when the SCIM operates between 0 to 0.2 slip, because the *x*-axis UMP produced by the 3-pole pair and 5-pole pair flux waves is opposite to each other (3 pole pair flux is leading and 5 pole-pair flux wave is lagging the rotor). Therefore, the small amount of stator winding harmonics flux wave will produce a more significant offset. For the difference between FEA and experimental results, the higher harmonics flux waves that crosses the air-gap might be different, as the leakage path is difficult to be predicted.

From the close correlation of both FEA and experimental results with the results calculated with the damping coefficient, the UMP Damping Coefficient can be verified. In addition, from the existence of *x*-axis UMP when the rotor eccentricity is set towards the *y*-axis direction, it can be concluded that the damping of UMP will slightly shift the direction of UMP away from the narrowest air-gap, and the direction is slip dependent.

6. UMP at different operating conditions

6.1. Excitation frequency

From (11), the counteracting flux wave produced by the cage rotor is a function of the slip frequency of the additional pole pair flux wave, where the slip frequency changes with the supply frequency.

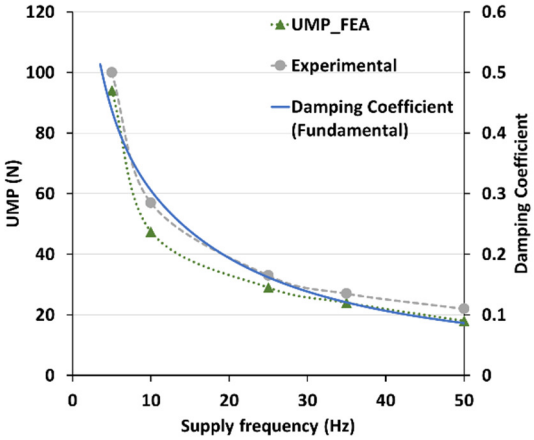

Fig. 15. *UMP and Damping Coefficient at different supply frequencies*

Fig. 15 shows the UMP of the 8-pole SCIM at different excitation frequencies. It was tested at no-load with 30% rated flux and 20% static eccentricity. V/F control is used in the test, as the magnitude of the stator flux-linkage can be maintained when using V/F control [30]. As the UMP damping effect of the fundamental magnetising flux is going to be investigated, the SCIM is run at no-load in the test, where the fundamental magnetising flux is the dominant flux at the air-gap for any excitation frequency.

As the magnitude of the magnetising flux is remained constant at different supply frequency, the change of UMP should be proportional to the UMP Damping Coefficient. This is because the damping coefficient is linearly proportional to the effective eccentricity of the machine, which is shown in (19).

Therefore, it is shown in Fig. 15 that the UMP is higher when the supply frequency is lower. In addition, the UMP Damping Coefficient shows good correlation with the UMP, which can also verified the proposed UMP Damping Coefficient.

6.2. Rotor resistance

As UMP Damping Coefficient is also a function of the rotor resistance, SCIM with different rotor resistance are investigated in this sub-section. The results are taken from FEA, where 20% static eccentricity is set for the 4-pole SCIM. Let the original rotor bar resistance as 1 p.u., the UMP of 3 different rotor bar resistance at rated voltage and frequency are shown in Fig. 16.

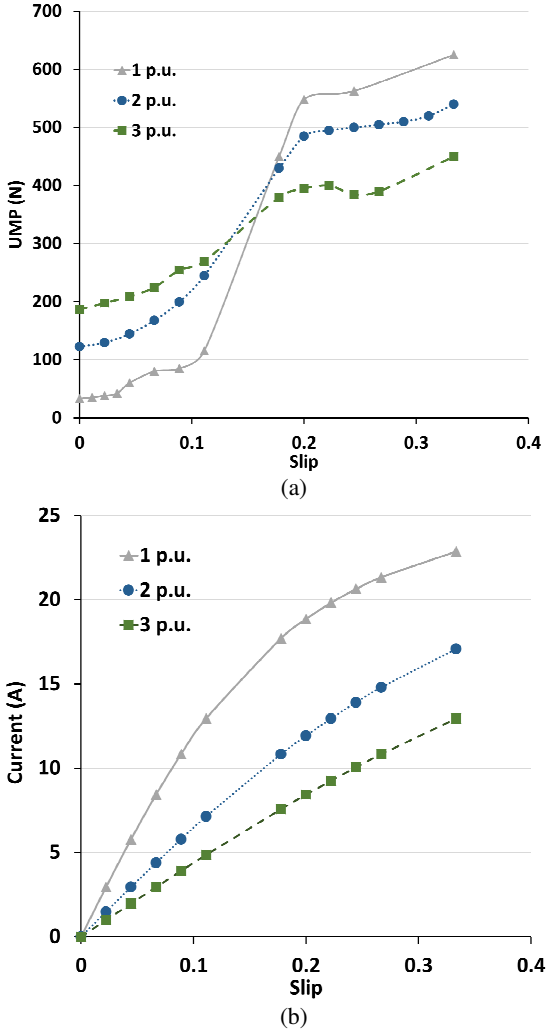

Fig. 16. *Different rotor bar resistance: (a) UMP (b) current*

Refer to Fig. 16, from 0 to 0.1 slip, 1 p.u. resistance has the lowest UMP while the 3 p.u. resistance has the highest UMP. This is because the damping effect is more significant for the rotor with lower resistance. As the magnetising flux is the dominant flux at low slip, the UMP is higher when the rotor resistance is higher.

Then, the difference of UMP becomes smaller when the slip increases because the air-gap leakage flux is not affected by the damping effect of the rotor bar. After 0.15 slip, the order of the UMP for each case is inversed, where the SCIM with 1 p.u. resistance has the highest UMP while the SCIM with 3 p.u. resistance has the lowest UMP. This s due to the induced current is lower for the SCIM with higher rotor bar resistance. The rotor phase current in the machine is illustrated in Fig. 16(b). As the current of the machine with 1 p.u. rotor resistance has the highest rate of increment, the UMP of the machine also had the highest rate of increment when the slip increases. This is because the contribution of air-gap leakage flux increases as the current increases, in which the increment of air-gap leakage flux generates a larger UMP.

7. Conclusions

Rotor eccentricity in electrical machines causes uneven magnetic flux distribution, whereby UMP is produced. However, parallel circuits in electrical machines damp the additional magnetic flux waves caused by rotor eccentricity. Although this effect had been raised by a number of researchers, it had not been quantitatively investigated. In this paper, the existence of the UMP damping effect is presented by comparing the SCIM and the WRIM, since the cage rotor bars of SCIMs are naturally parallel-connected, and the rotor winding configuration of WRIMs is pole-specific.

When rotor eccentricity occurs, the SCIM has a much more evenly distributed magnetic flux than the WRIM; hence the UMP of the SCIM is much smaller than the WRIM. Moreover, the difference in UMP between the two rotor types changes with slip, as UMP damping is a function of rotor slip. For example, the damping of UMP of a 4-pole-pair SCIM is least effective at 0.2 rotor slip. This is because the 5-pole-pair flux wave, which is caused by the rotor eccentricity, does not induce current in the rotor bars when the machine is running at 0.2 slip.

To find the UMP damping effect, the derivation of the damping of UMP is shown in this paper. A UMP damping coefficient is also proposed to represent the UMP reduction percentage, which is verified using both FEA and experimental work. The effective eccentricity is also proposed to be used in the UMP calculation, where the it is a product of the degree of rotor eccentricity and the UMP damping coefficient. Traditionally, numerical methods need to be used to calculate the UMP of SCIMs because of the existence of circulating current in the rotor bars. As the circulating current had already been included in the UMP damping coefficient, the UMP can be calculated analytically using the proposed effective eccentricity.

Lastly, the UMP at different excitation frequencies and rotor resistance are investigated, as these are the parameters that affect the UMP damping effect. The SCIM with higher excitation frequency has a smaller UMP when it is not loaded. Meanwhile, the SCIM with higher rotor resistance has a larger UMP when it operates below its rated slip. However, as the slip increases, the SCIM with lower rotor resistance has a larger UMP, as lower rotor resistance would lead to higher rotor currents.

8. References

[1] W. R. Finley, M. M. Hodowanec and W. G. Holter, "An analytical approach to solving motor vibration problems," Industry Applications Society Annual Petroleum and Chemical Technical Conference, San Diego, CA, USA, 1999, pp. 217-232.

[2] J. Faiz, B. M. Ebrahimi and M. B. B. Sharifian, "Different Faults and Their Diagnosis Techniques in Three-Phase Squirrel-Cage Induction Motors—A Review", Electromagnetics, 2006, pp. 543-569

[3] W. T. Thomson and A. Barbour, "On-line current monitoring and application of a finite element method to predict the level of static airgap eccentricity in three-phase induction motors," IEEE Transactions on Energy Conversion, vol. 13, no. 4, pp. 347-357, Dec. 1998.

[4] J. K. H. Shek, D. G. Dorrell, M. Hsieh, D. E. Macpherson and M. A. Mueller, "Reducing bearing wear in induction generators for wave and tidal current energy devices," IET Conference on Renewable Power Generation, Edinburgh, 2011, pp. 1-6.

[5] J. R. Cameron, W. T. Thomson and A. B. Dow, "Vibration and current monitoring for detecting airgap eccentricity in large induction motors," IEE Proceedings B - Electric Power Applications, vol. 133, no. 3, pp. 155-163, May 1986.

[6] S. Nandi, H. A. Toliyat and X. Li, "Condition monitoring and fault diagnosis of electrical motors-a review," in IEEE Transactions on Energy Conversion, vol. 20, no. 4, pp. 719-729, Dec. 2005.

[7] J. Faiz, I. T. Ardekanei and H. A. Toliyat, "An evaluation of inductances of a squirrel-cage induction motor under mixed eccentric conditions," IEEE Transactions on Energy Conversion, vol. 18, no. 2, pp. 252-258, Jun. 2003.

[8] P. J. Tavner, "Review of condition monitoring of rotating electrical machines," IET Electric Power Applications, vol. 2, no. 4, pp. 215-247, Jul. 2008.

[9] D. G. Dorrell, J. Shek, M. Hsieh and M. A. Mueller, "Unbalanced Magnetic Pull in Cage Induction Machines for Fixed-Speed Renewable Energy Generators," IEEE Transactions on Magnetics, vol. 47, no. 10, pp. 4096-4099, Oct. 2011.

[10] A. Salah, Y. Guo and D. Dorrell, "Monitoring and damping unbalanced magnetic pull due to eccentricity fault in induction machines: A review," 20th International Conference on Electrical Machines and Systems, Sydney, NSW, 2017, pp. 1-6.

[11] H. Frohne, "Einseitigen magnetischen Zugkrafte in Drehstrommaschinen," ETZ-A, vol. 83, no. 10, pp. 299-303, 1962

[12] A. Stavrou and J. Penman, "Modelling dynamic eccentricity in smooth air-gap induction machines," IEMDC 2001. IEEE International Electric Machines and Drives Conference, Cambridge, MA, USA, 2001, pp. 864-871.

[13] D. G. Dorrell, J. K. H. Shek and M. Hsieh, "The Development of an Indexing Method for the Comparison of Unbalanced Magnetic Pull in Electrical Machines," IEEE Transactions on Industry Applications, vol. 52, no. 1, pp. 145-153, Jan.-Feb. 2016.

[14] D. G. Dorrell, J. K. H. Shek, M. A. Mueller, M. Hsieh, "Damper Windings in Induction Machines for Reduction of Unbalanced Magnetic Pull and Bearing Wear," IEEE Transaction on Industry Applications, vol. 49, no. 5, pp. 2206,2216, Sep.-Oct. 2013.

[15] M. Bradford, "Unbalanced Magnetic pull in a 6-pole induction motor," Proceedings of Institution of Engineers, vol.115, no. 11, pp. 1619-1627, Nov. 1968.

[16] A. Burakov, A. Arkkio, "Comparison of the Unbalanced Magnetic Pull Mitigation by the Parallel Paths in the Stator and Rotor Windings," IEEE Transactions on Magnetics, vol. 43, no. 12, pp. 4083-4088, Dec. 2007.

[17] D. G. Dorrell and A. C. Smith, "Calculation of UMP in induction motors with series or parallel winding connections," IEEE Transactions on Energy Conversion, vol. 9, no. 2, pp. 304-310, Jun. 1994.

[18] M. Wallin, M. Ranlof and U. Lundin, "Reduction of Unbalanced Magnetic Pull in Synchronous Machines due to Parallel Circuits," in IEEE Transactions on Magnetics, vol. 47, no. 12, pp. 4827-4833, Dec. 2011.

[19] P. Frauman, A. Burakov and A. Arkkio, "Effects of the Slot Harmonics on the Unbalanced Magnetic Pull in an Induction Motor With an Eccentric Rotor," in IEEE Transactions on Magnetics, vol. 43, no. 8, pp. 3441-3444, Aug. 2007.

[20] H. Chuan and J. K. H. Shek, "Calculation of unbalanced magnetic pull in induction machines through empirical method," IET Electric Power Applications, vol. 12, no. 9, pp. 1233-1239, 11 2018.

[21] D. G. Dorrell and M. F. Hsieh, "Calculation of Radial Forces in Cage Induction Motors at Start—The Effect of Rotor Differential," IEEE Transactions on Magnetics, vol. 46, no. 8, pp. 3029-3032, Aug. 2010.

[22] S. Nandi, "Modeling of induction machines including stator and rotor slot effects," in IEEE Transactions on Industry Applications, vol. 40, no. 4, pp. 1058-1065, July-Aug. 2004.

[23] D. G. Dorrell, "Sources and characteristics of unbalanced magnetic pull in 3-phase cage induction motors with axial-varying rotor eccentricity," IEEE Energy Conversion Congress and Exposition, San Jose, CA, 2009, pp. 240-247.

[24] D. Guo, F. Chu, D. Chen, "The unbalanced magnetic pull and its effects on vibration in a three phase generator with eccentric," Journal of Sound and Vibration, vol. 254, no. 2, 2002, pp. 297-312, Jul. 2002.

[25] A. C. Smith and D. G. Dorrell, "Calculation and measurement of unbalanced magnetic pull in cage induction motors with eccentric rotors. I. Analytical model," IEE Proceedings - Electric Power Applications, vol. 143, no. 3, pp. 193-201, May 1996.

[26] H. Chuan and J. K. H. Shek, "Reducing Unbalanced Magnetic Pull of an induction machine through active control," IET International Conference on Power Electronics, Machines and Drives, Glasgow, 2016, pp. 1-6.

[27] T. W. Preston, A. B. J. Reece and P. S. Sangha, "Induction motor analysis by time-stepping techniques," IEEE Transactions on Magnetics, vol. 24, no. 1, pp. 471-474, Jan. 1988.

[28] D. Howe and Z. Q. Zhu, "The influence of finite element discretisation on the prediction of cogging torque in permanent magnet excited motors," IEEE Transactions on Magnetics, vol. 28, no. 2, pp. 1080-1083, Mar. 1992.

[29] I. Tsukerman, "Accurate computation of 'ripple solutions' on moving finite element meshes," IEEE Transactions on Magnetics, vol. 31, no. 3, pp. 1472-1475, May 1995.

[30] A. Munoz-Garcia, T. A. Lipo and D. W. Novotny, "A new induction motor V/f control method capable of high-performance regulation at low speeds," IEEE Transactions on Industry Applications, vol. 34, no. 4, pp. 813-821, July-Aug. 1998.